Available online at www.sciencedirect.com

ScienceDirect

Procedia CIRP 78 (2018) 161–165

www.elsevier.com/locate/procedia

6th CIRP Global Web Conference
"Envisaging the future manufacturing, design, technologies and systems in innovation era"

Correlation between process load and deep rolling induced residual stress profiles

Denkena, B.[a], Grove, T.[a], Breidenstein, B.[a], Abrão, A.[b], Meyer, K.[a]*

[a]*Institute of Production Engineering and Machine Tools, Leibniz Universität Hannover, 30823 Garbsen, Germany*
[b]*Departement of Mechanical Engineering, Universidade Federal de Minas Gerais, 31270-901 Belo Horizonte, Brazil*
** Corresponding author. Tel.: +49 511 762-18269; fax: +49 511 762-5115. E-mail address: meyer@ifw.uni-hannover.de*

Abstract

Deep rolling is often used as a finishing step after cutting because of its beneficial influence on surface and subsurface properties, which lead to an increase in performance and lifecycle behavior. This manufacturing process is suitable to reduce roughness and to induce compressive residual stresses. As thermal effects only play a minor role in the deep rolling process, it is possible to link the resulting residual stresses to the analytically determined internal process loads. The boundaries of these relationships are investigated on hardened AISI 4140 using different mechanical loads and overlap factors.

Keywords: Residual stresses, deep rolling, mechanical load, surface integrity

1. Introduction

Nomenclature

a_p	depth of cut [mm]
d_b	ball diameter [mm]
d_w	workpiece diameter [mm]
f	feed [mm]
F_w	deep rolling force [N]
p	deep rolling pressure [MPa]
p_0	maximal pressure [MPa]
r_k	radius of contact [mm]
u	overlap factor [-]
v_c	cutting speed [m/min]
v_r	tool speed during deep rolling [m/min]
η	efficiency coefficient of the compressor system
φ	angle of measurement direction [°]
$\sigma_{eq,max}$	maximum equivalent stress [MPa]
σ_1	principal residual stress [MPa]
σ_2	stress perpendicular to the principal stress [MPa]

1.1 Deep rolling and its influence on workpiece properties

Residual stresses significantly influence the functional behaviour of a machined component including static and dynamic strength. Due to thermal and mechanical loading, relaxation of residual stresses decreases their effect [1,2]. Compressive residual stresses show beneficial effects on the fatigue strength of metallic alloys. These positive effects, as well as other properties, can be altered by surface treatment. Common used techniques are laser peening, deep rolling or shot peening [3]. Juijerm and Altenberger compared influenced surface and subsurface properties, i.e. the induced first order residual stresses, dislocation densities, increase of

10.1016/j.procir.2018.09.063

microhardness and surface roughness of machined parts using laser peening, deep rolling and shot peening. This comparison resulted in a comparable maximal residual stress of all three methods and a beneficial roughness (Rz < 1 µm under certain conditions) using deep rolling processes [4]. The resulting effects of deep rolling on hardened AISI 1060 are reported by Abrão et al. [5]. The underlying principle of grain refinement,

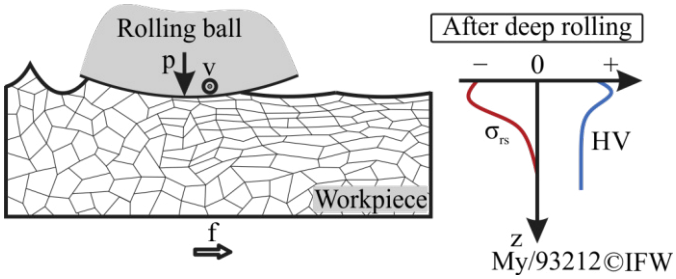

Figure 1: Influence of deep rolling on subsurface properties [1]

flattening of roughness peaks and the residual stress state is depicted in Figure 1. For modification of rotational symmetric workpieces, deep rolling using hydrostatic tools can also provide economic benefits compared to laser or shot peening. Because it is possible to mount these tools on a conventional lathe, no transfer to external machines is necessary [6]. Newer research and industrial practice lead to the development of a combined turning and deep rolling tool. Using these tools has economic and quality advantages because it removes the additional deep rolling step and improves the surface quality. When processing hardened steels using this hybrid tool, it is possible to adjust the relative position of the ceramic rolling ball to the cutting edge and therefore smoothen the roughness peaks created by the turning process [7, 8]. An additional benefit lies in the turning-induced process heat, which creates a similar effect to deep rolling at elevated temperatures as performed by Juijerm and Altenberger [9].

1.2 Internal mechanical load and its influence on residual stresses

The formation of residual stresses during machining is influenced by the magnitude of thermal and mechanical loads. Because most manufacturing processes generate both, thermal and mechanical loads, the predictability of residual stresses induced by manufacturing processes is only possible on a limited scale. The ability of leading research institutes to induce targeted residual stresses was tested in a *Round Robin collaborative work* by Jawahir et al. [2]. This test showed a high deviation when comparing the machined parts to the target value. The low predictability of residual stresses leads to the use of mainly empiric models that may show a high accuracy for the tested cases but have a low general validity. In the last years, researchers worked on methods to predict the surface integrity by changing the perspective from the simple description of process parameters (i.e. feed, cutting speed) to the thermal, mechanical and chemical loads [10]. Meyer & Kämmler investigated the influence of the deep rolling process on the induction of residual stresses [11]. They used the information of the external load (deep rolling force) to calculate the internal load of the workpiece. As chemical and thermal aspects can be neglected, the load can be assumed to be only mechanic. Therefore, they approximated the maximum equivalent stresses $\sigma_{eq,max}$ using Hertzian equations according to Johnson [12]. While this approach is not new and has been performed previously [13], the novelty lies in the comparison between the maximum equivalent stress and the maximum residual stress. By using different ball diameters (d_{b1} = 6 mm, d_{b2} = 13 mm) of the deep rolling tool, they select the deep rolling forces F_w to match $\sigma_{eq,max}$ for both ball diameters. This leads to similar residual stress magnitudes for both ball diameters. However, this research leaves open, if it is possible to determine the depth information of this maximum. The influence of the feed/overlap on the resulting residual stress profile is also uncertain. Because the contact area between workpiece and tool differs with changing process loads, it is useful to use the overlap factor instead of the feed to compare the contact area between the deep rolling tool and the workpiece [8]. The overlap factor is a unitless factor, which describes the relation between workpiece material that has been in contact with the deep rolling tool and material without contact, as depicted in Figure 2. A negative overlap results in unmachined material.

The contact radius can be calculated using Hertzian contact mechanics under the assumption of a contact between spheres, r and E are calculated according to [12,13]:

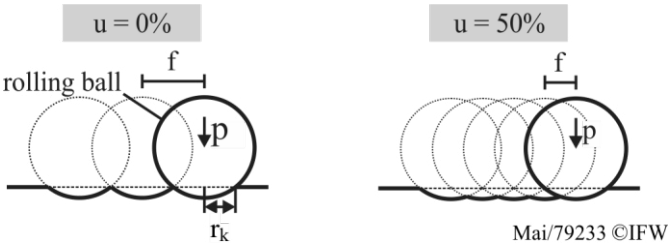

Figure 2: Schematic explanation of the overlap factor u

$$r_k = \sqrt[3]{\frac{3\cdot(1-\nu^2)\cdot r\cdot F_w}{2\cdot E}} \quad (1)$$

Using a rotating workpiece, the overlap factor can be calculated by:

$$u = 1-\frac{f}{2\cdot r_k} \quad (2)$$

In summary, there are still further investigations needed concerning the comparability of maximum equivalent stresses on materials with different mechanical characteristics. The influence of the feed and the overlap factor is not tested yet, and there is no knowledge of the predictability of the depth of the residual stress maximum using the internal load. Therefore, this paper uses Hertzian contact mechanics to compare internal loads and residual stress depth distributions on hardened AISI4140. There will also be variations of the overlap factor u and on the deep rolling pressure p.

2. Experimental setup

The experiments were conducted using a CNC-controlled Gildemeister CTX 520 L lathe. The cylindrical workpieces are made of AISI 4140, which has been quenched and tempered to a hardness of 50 HRc. The workpiece diameter is 59 mm. Because of the heat treatment induced corrosion, the samples were prepared by turning using SNMN 12048 carbide inserts with v_c = 100 m/min, a_p = 0.25 mm and f = 0.1 mm. The deep rolling experiments were performed using an ECOROLL HG6 tool with a ball diameter of d_b = 6.35 mm. The pressure p was varied between 5 to 40 MPa in four steps. The feed was chosen to achieve overlap factors of u = -0.15, 0.55, 0.78. For the initial planning, the deep rolling force F_w was estimated by:

$$F_w = p \cdot \left(\frac{d_b}{2}\right)^2 \cdot \pi \quad (3)$$

Because of systematic losses of the compressor system, the resulting force decreases. Therefore, the forces were measured by using a Kistler 9121 dynamometer, as depicted in Figure 3, to determine the efficiency of the compressor system. Based on the theoretic deep rolling force, the contact radius is calculated according to (1). The process parameters are depicted in Table 1. Using four pressure steps and three overlap factors, a total of 12 samples was machined.

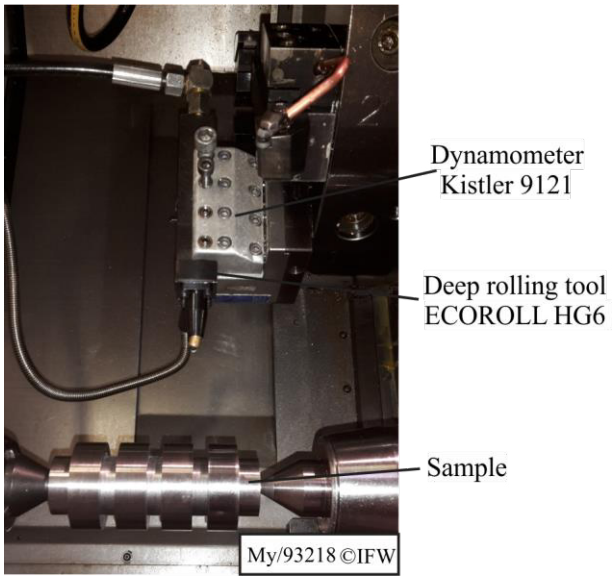

Figure 3: Experimental setup

After the deep rolling experiments, the residual stress depth profiles were determined using a Seiffert XRD3000P X-Ray diffractometer using CrKα radiation. This diffractometer can reach an accuracy of ± 10 MPa on ferrous materials under ideal conditions (flat surface, small grain size, no texture). These conditions are not fulfilled for the used samples, because they have a curved surface and after deep rolling, a texture has to be expected. Therefore, a lower accuracy is expected. The measurements have been performed using three angles in relation to the radial direction (φ = 0°, 45°, 90°) to determine the principle stress and its direction. The depth information was gathered using electrochemical polishing to remove material layers.

Table 1: Parameters based on theoretical deep rolling force $F_{w,th}$

p [MPa]	$F_{w,th}$ [N]	r_k [mm]	$\sigma_{eq,max,th}$ [MPa]	u_{th} [-]
5	158	0.1303	4452.4	-0.15; 0.55; 0.78
10	316	0.1642	5609.7	-0.15; 0.55; 0.78
30	950	0.2368	8090.5	-0.15; 0.55; 0.78
40	1276	0.2606	8904.8	-0.15; 0.55; 0.78

3. Results

3.1. Efficiency of the compressor system

Figure 4 shows the measured deep rolling forces in comparison to the theoretical forces. The forces were measured with three repetitions for every pressure stage. The deviation was in a range of ± 5 N. Error bars would therefore not be visible in the figure.

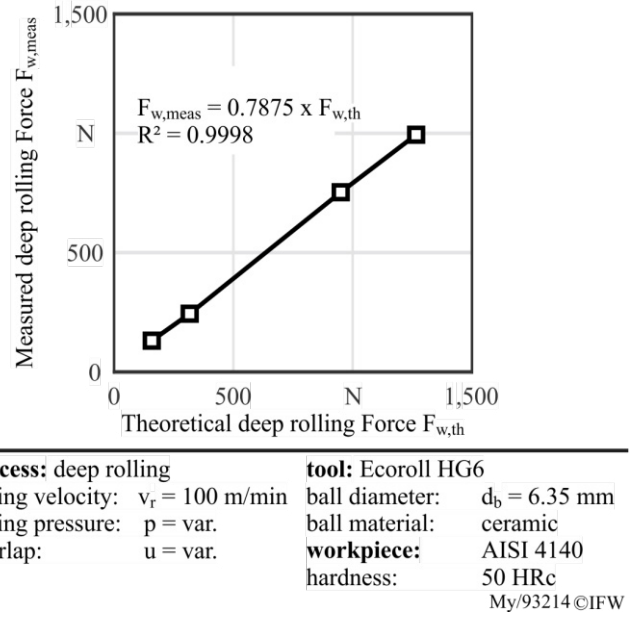

Figure 4: Comparison of theoretical and measured deep rolling forces

This measurement shows an efficiency of η = 0.7875 for the compressor system. The deviation between theoretical and measured forces also causes changes regarding the process load, the radius of contact and the resulting overlap depicted in Table 1. The resulting new parameters are shown in Table 2.

Table 2: Process parameters based on measured F_w

p [MPa]	$F_{w,meas}$ [N]	r_k [mm]	$\sigma_{eq,max}$ [MPa]	u [-]
5	131	0.1202	2486.6	-0.22; 0.5; 0.75
10	244	0.1512	3052.0	-0.22; 0.5; 0.75
30	763	0.2191	4463.1	-0.22; 0.5; 0.75
40	994	0.2404	4877.4	-0.22; 0.5; 0.75

3.2. Influence of the overlap factor u on the residual stress-depth distribution

One aim of this paper is to determine the influence of the overlap factor u on the residual stresses. Figure 5 shows the residual stress depth in the three measured directions ($\sigma_{\varphi=0°}$, $\sigma_{\varphi=45°}$, $\sigma_{\varphi=90°}$) and the principal stresses (σ_1, σ_2) for a deep rolled sample using p = 5 MPa and u = -0.22. It is visible, that the principal residual stresses match $\sigma_{\varphi=0°}$ and $\sigma_{\varphi=90°}$ with minor deviations. This result is representative for all measured samples. Therefore, the following analysis uses the principal stresses.

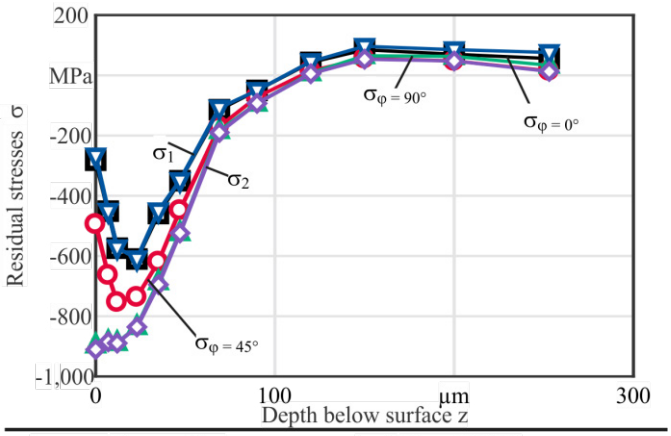

Figure 5: Residual stress-depth distribution

The maximum equivalent stress $\sigma_{eq,max}$ was calculated according to Hertz [12]. The contact is estimated as a sphere-sphere contact, which is the closest possible approximation [14]. Considered here are the measured forces, the workpiece and tool diameters and the material properties of the workpiece and the tool. The tool parameters are chosen based on the specifiactions given by the manufacturer. The workpiece parameters are estimated based on the data sheet. The used parameters are listed in Table 3.

Table 3: Parameters used for the calculation of $\sigma_{eq,max}$

Property	Tool	Workpiece
Diameter	d_b = 6.35 mm	d_w = 59 mm
Young's modulus	E = 420 GPa	E = 210 GPa
Poisson Ratio	ν = 0,3	ν = 0,3

Figure 6 shows the influence of the overlap factor on the relation between the maximum equivalent stress and the maximum of the residual stresses without information of the depth. The graph on the left illustrates the influence on the principle stress while the right shows the influence on σ_2. While the results for the positive overlap factors show similar trends, especially regarding the perpendicular stress, the negative overlap factor of u = -0.22 deviates. In general, the form of the trend lines differs from those determined by Meyer & Kämmler [11]. A possible explanation could lie in the heat treatment induced ([11]: 27 HRc, this paper 50 HRc) different mechanical properties. Because the heat treatment does not only influence hardness but also the yield $R_{p0.2}$ and maximum tensile strength R_m, the relationship between $\sigma_{eq,max}$ and these values changes. With the resulting higher yield strength of the samples used in this paper, it is also possible to induce higher residual stresses.

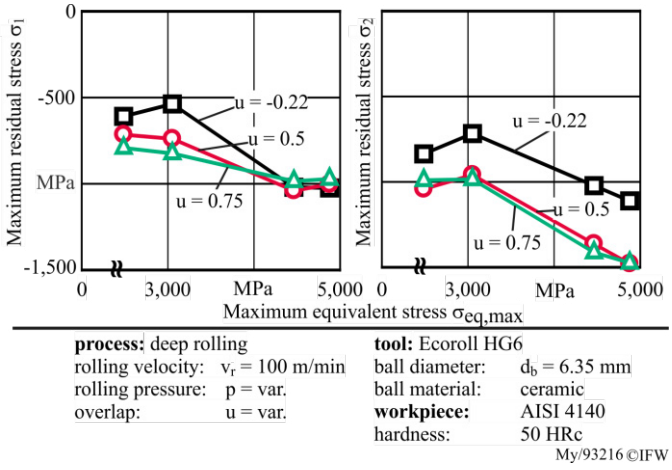

Figure 6: Comparison between the $\sigma_{eq,max}$ and the principle stresses

However, these results show, that a certain overlap factor is necessary to reach a stable introduction of residual stresses. It is necessary to perform further experiments to find the lowest necessary overlap. It should also be mentioned, that a negative overlap factor is unrealistic and would not be performed in a production scenario, because the surface roughness would have a high magnitude.

3.3. Comparison of the depth information and shear stresses

In the last paragraph, the maximal residual stresses were correlated to the maximal equivalent stresses. This knowledge could for example be used to predict the maximal residual stresses when using different ball sizes. However, these processes would still produce differences in the depth of this residual stress maximum. The possibility to additionally adjust the position residual stress maximum is a key step towards the adaption of the surface integrity to different load scenarios. The shear stress τ is calculated according to Johnson [12, 15]:

$$\sigma_{zz} = -p_0\left(1+\frac{z^2}{r_k^{\,2}}\right) \tag{4}$$

$$\sigma_{yy} = -p_0\left[(1+\nu)\left(1-\frac{z}{r_k}\cdot\tan^{-1}\frac{r_k}{z}\right)-\frac{1}{2}\left(1+\frac{z^2}{r_k^{\,2}}\right)\right]^{-1} \tag{5}$$

$$\tau = \left|\sigma_{zz}-\sigma_{yy}\right| \tag{6}$$

When considering τ in comparison to σ_2, the principle stress, as depicted in Figure 7, it can be seen that the maximum shear

stress is in a depth position near the residual stress. However, the overlap factor u also influences the position of the residual stress maximum.

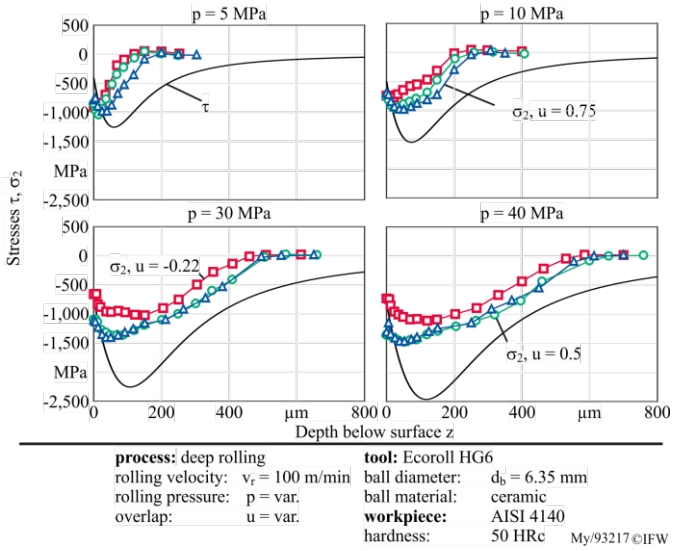

Figure 7: Comparison between the distribution of shear and residual stresses

From this data, it can be considered, that it is possible to estimate the residual stress maximum by calculating the shear stress τ and using its maximum. However, a variation of the overlap factor alongside with the variation of the deep rolling pressure leads to a variation of the resulting residual stress-depth profile – especially for the lower pressure stages (p = 5 MPa, p = 10 MPa). This should be considered for the design of deep rolling processes.

4. Conclusions and outlook

The aim of this research lies in the description of residual stresses based on the internal process loads of the deep rolling process. Additional information is gained by the consideration of systematic losses of the compressor system, which improves the accuracy of the analytic prediction of the deep rolling force F_w. Also observed is the influence of the overlap factor u on the process signature of deep rolling processes. It is shown, that this factor should also be considered as an influence on the resulting residual stress. It was also shown, that the maximum shear stresses τ has a similar distance to the surface as the residual stress maximum.
These findings are gained using a ball diameter of d_b = 6.35 mm. Additional research should be performed using different ball diameters d_b in order to prove the generality of these findings. The knowledge of the magnitude and position of the residual stress maximum based on the process load can be used to tailor the manufacturing according to the load during the lifecycle of the machined part.

5. Acknowledgements

The authors would like to thank the German (DFG) and the Brazilian Research Foundation (CAPES) for funding the BRAGECRIM collaboration project “Influence of the manufacturing process on the subsequent residual stress relaxation in AISI 4140 steel”.

References

[1] Schulze V. Modern Mechanical Surface Treatment: States, Stability, Effects. Weinheim: Wiley-VCH; 2006.
[2] Jawahir IS, Brinksmeier E, M'Saoubi R, Aspinwall DK, Outeiro JC, Meyer D et al. Surface integrity in material removal processes: Recent advances. CIRP Annals 2011;60(2):603–26.
[3] Delgado P, Cuesta II, Alegre JM, Díaz A. State of the art of Deep Rolling. Precision Engineering 2016;46:1–10.
[4] Juijerm P, Altenberger I. Fatigue Performance Enhancement of Steels using Mechanical Surface Treatments. Journal of Metals, Materials and Minerals 2007(17).
[5] Abrão AM, Denkena B, Köhler J, Breidenstein B, Mörke T. The inducement of residual stress through deep rolling of AISI 1060 steel and its subsequent relaxation under cyclic loading. Int J Adv Manuf Technol 2015;79(9-12):1939–47.
[6] Rodríguez A, López de Lacalle LN, Celaya A, Lamikiz A, Albizuri J. Surface improvement of shafts by the deep ball-burnishing technique. Surface and Coatings Technology 2012;206(11-12):2817–24.
[7] Denkena B, Poll G, Maiß O, Pape F, Neubauer T. Enhanced boundary zone rolling contact fatigue strength through hybrid machining by hard turn-rolling. Bearing World Journal 2016;1:87–102.
[8] Denkena B, Grove T, Maiss O. Influence of Hard Turned Roller Bearings Surface on Surface Integrity after Deep Rolling. Procedia CIRP 2016;45:359–62.
[9] Juijerm P, Altenberger I. Effect of high-temperature deep rolling on cyclic deformation behavior of solution-heat-treated Al–Mg–Si–Cu alloy. Scripta Materialia 2007;56(4):285–8.
[10] Brinksmeier E, Klocke F, Lucca DA, Sölter J, Meyer D. Process Signatures – A New Approach to Solve the Inverse Surface Integrity Problem in Machining Processes. Procedia CIRP 2014;13:429–34.
[11] Meyer D, Kämmler J. Surface Integrity of AISI 4140 After Deep Rolling with Varied External and Internal Loads. Procedia CIRP 2016;45:363–6.
[12] Johnson KL. Contact mechanics. Cambridge University Press; 1985.
[13] Klocke F, Liermann J. Roller burnishing of hard turned surfaces. International Journal of Machine Tools and Manufacture 1998;38(5-6):419–23.
[14] Röttger K. Walzen hartgedrehter Oberflächen. phD-Dissertation. Aachen: Shaker; 2003.
[15] Popov VL. Kontaktmechanik und Reibung: Von der Nanotribologie bis zur Erdbebendynamik 2010.